

MIMIC-SR-ICD11: A Dataset for Narrative-Based Diagnosis

Yuxin Wu

University of Memphis, Unite State

YWU10@MEMPHIS.EDU

Shiqi Wang

The Second Clinical College of Guangzhou University of Chinese Medicine, China

20251110858@STU.GZUCM.EDU.CN

Vasile Rus

University of Memphis, Unite State

VRUS@MEMPHIS.EDU

Abstract

Disease diagnosis has become a central pillar of modern healthcare, enabling early detection and timely intervention for acute conditions while guiding lifestyle adjustments and medication regimens to prevent or slow chronic disease. Self-reports preserve clinically salient signals that templated electronic health record (EHR) documentation often attenuates or omits, especially subtle but consequential details. To operationalize this shift, we introduce MIMIC-SR-ICD11, a large English diagnostic dataset built from EHR discharge notes and natively aligned to WHO ICD-11 terminology. We further present LL-Rank, a likelihood based re-ranking framework that compute a length normalized joint likelihood of each label under the clinical report context and subtracting the corresponding report free prior likelihood of that label. On seven model backbones, LL-Rank consistently outperforms a strong generation + mapping baseline (GenMap). Ablation experiments reveal that LL-Rank's improvement mainly arises from its PMI-based scoring, which isolates semantic compatibility from label frequency bias.

Keywords: Clinical NLP, Disease Prediction, Patient Self-Reports

Data and Code Availability Code is available at <https://github.com/woqingdoua/MIMIC-SR-ICD11>. Data use de-identified MIMIC-IV/MIMIC-IV-Note under PhysioNet credentialled access; our generated self-reports are released for research-only use.

Institutional Review Board (IRB) This study did not involve human subjects or identifiable private information and therefore did not require IRB approval.

1. Introduction

Disease diagnosis has become a central pillar of modern healthcare, enabling early detection and timely intervention for acute conditions, while also guiding lifestyle adjustments and medication regimens to prevent or slow chronic diseases. It is particularly valuable in resource-limited environments and helps individuals without medical expertise avoid a long search for the right provider.

More recently, large language models (LLMs) have demonstrated strong performance on clinical question–answering benchmarks [Singhal et al. \(2023, 2025\)](#). These models are typically fine-tuned on exam-style question–answer datasets designed for medical students [Jin et al. \(2020\)](#); [Pal et al. \(2022\)](#); [Jin et al. \(2019\)](#), but their training regime does not directly translate to real-world diagnostic workflows, since exam-style benchmarks present well-defined questions with fixed answer options, whereas clinical diagnosis requires interpreting ambiguous, multi-symptom narratives. Datasets for automatic diagnosis such as DX [Xu et al. \(2019\)](#) and DDXPlus [Fansi Tchang et al. \(2022\)](#) rely on categorical symptom indicators. This representation obscures important clinical detail—for example, reducing “severe, intermittent chest pain radiating to the left arm” to a present/absent flag loses information about intensity and distribution—and, because these collections are built for fixed-label classification, models trained on them cannot readily incorporate new symptoms or expand beyond the original disease set. Su et al. [Su et al. \(2024\)](#) take a step toward free-text inputs with patient-authored symptom descriptions, but their dataset is confined to Chinese and leaves English self-reports unexplored.

Taken together, these limitations motivate a shift toward inputs that mirror how patients present symptoms at first contact: patient-authored self-reports.

Self-reports can be collected online before a visit and are well suited to telemedicine, longitudinal follow-up, and population screening. They are especially effective for early triage and first-contact routing, and they generalize across front-end applications such as online triage tools, navigation assistants, and conversational agents. Critically, self-reports preserve clinically salient detail that templated EHR documentation often attenuates or omits (e.g. the time course of illness, subjective experience (pain intensity, triggers and relievers), subtle yet important co-occurring symptoms). Training and evaluating on self-reports therefore better matches deployment conditions and captures information that categorical checklists or templated notes tend to suppress.

To operationalize this shift, we introduce an English-language dataset, MIMIC-SR-ICD11, which converts EHR discharge notes into first-person patient self-reports and standardizes diagnoses using WHO ICD-11 terminology. Building on the advantages of a unified label space, we propose LL-Rank, a likelihood-based re-ranking method that combines the conditional likelihood of each ICD-11 label given the report with an explicit corpus-derived prior. By balancing textual evidence with label priors, LL-Rank yields better-calibrated rankings and consistently improves performance, with particularly strong gains on short-token labels.

2. Data Construction

We built the dataset on the latest MIMIC-IV [Johnson et al. \(2024\)](#) and MIMIC-IV-Note [Johnson et al. \(2022\)](#) releases. The construction pipeline consists of two steps, with the workflow shown in Fig. 2. First, we map ICD-9 and ICD-10 diagnoses from MIMIC-IV to ICD-11 terminology. Second, we retrieve free-text symptom descriptions from the MIMIC-IV-Note EMR notes and rewrite them as first-person patient self-reports.

2.1. Diagnosis Mapping

We derive diagnostic labels from MIMIC-IV and retain only the primary diagnosis. Each record carries an ICD code and a version flag. For encounters coded in ICD-9, we first convert to ICD-10 using the U.S. Centers for Medicare & Medicaid Services (CMS) official FY2018 General Equivalence Mappings (GEMs)¹.

In this step, we keep only entries that are both “exact” and “mappable” in the GEMs metadata. We then enforce a one-to-one constraint at the code level. ICD-9 codes that map to multiple ICD-10 candidates are withheld for manual review rather than automatically converted.

Next, for all rows with an ICD-10 code (either originally ICD-10 or obtained from the previous step), we map to ICD-11 using the World Health Organization’s official mapping tables provided via the ICD-11 Browser ². We again retain only one-to-one correspondences to preserve semantic precision. After automatic mapping, approximately 10% of diagnoses are fully resolved. The remainder are curated by medically trained annotators who select the most faithful ICD-11 entity by consulting the source descriptor and validating candidates in the ICD-11 browser. During curation we exclude non-disease concepts (e.g., symptom/sign-only entries, aftercare, external causes) and overly broad or ambiguous categories to ensure labels represent clinically actionable diseases.

2.2. Patient’s self-report generation

The MIMIC-IV-Note dataset provides de-identified free-text hospital records for each patient, which typically include a mix of symptom descriptions, examination results, medical history, and social background information. To derive patient-style narratives suitable for large language model reasoning, we used ChatGPT³ (gpt-4o-mini) to convert these clinical notes into first-person self-reports. Before large-scale generation, our medical students curated a small development set of 10 notes and prompt-tuned the instruction (i.e., iteratively refined the wording and few-shot exemplars) so that the model reliably transforms EHR notes into patient-style narratives. During conversion, the prompt explicitly instructs the model to filter out clinician-generated content (physical examination findings, diagnostic test results, and professional assessments) and to retain only subjective symptom descriptions as recounted by the patient. The resulting self-reports are written in natural language using complete sentences from the patient’s perspective, which better aligns the input with real-world patient narratives and facilitates downstream disease diagnosis.

1. <https://www.cms.gov/medicare/coding-billing/icd-10-codes>

2. <https://icd.who.int/browse/2025-01/mms/en>
3. <https://openai.com/api/>

3. Method

3.1. Setup and Notation

Let x denote a patient self-report and let $\mathcal{C} = \{c_j\}_{j=1}^M$ be the fixed candidate set of ICD-11. We fine-tune LLMs with supervised fine-tuning (SFT) and LoRA adapters, then keep the adapted model θ for inference. Given a patient’s report, we wish to rank \mathcal{C} and evaluate top- k predictions.

3.2. Method 1: Greedy generation + label mapping (GenMap)

We first prompt the model θ to generate a short diagnostic phrase using deterministic greedy decoding. The resulting text is then mapped to the closest disease name from a fixed candidate list. To measure closeness, we compute token-level overlap between the generated phrase and each candidate label after tokenization. Each shared token contributes inversely to its overall frequency in the label corpus, so rarer and thus more informative tokens receive higher weight.

Candidates are ranked by a two-part key: (1) the number of overlapping tokens, and (2) the weighted rarity score used to break ties. This procedure favors candidates sharing distinctive terms with the generated text while de-emphasizing common medical words such as “disease” or “unspecified.” Sorting all candidates by this key yields a complete ranking, denoted GenMap. We report standard retrieval metrics including Hit@ k and Macro-F1@ k based on the top- k predictions.

3.3. Method 2: PMI-style Scoring (LL-Rank)

Rather than decoding a free string, we directly score each diagnosis candidate $c \in \mathcal{C}$ with a Pointwise Mutual Information (PMI) style criterion. PMI measures how much knowing x changes the likelihood of c . Using PMI rather than $\log p(c | x)$ alone discounts labels that are a priori frequent, thereby focusing the score on compatibility with the input rather than corpus popularity.

Given a candidate label c with tokenization $\tau(c) = y_{1:T(c)}$ and a fixed textual prompt `prefix`, we score it by the conditional per-token negative log-likelihood $\mathcal{L}_{\text{cond}}(x, c)$. By the autoregressive factorization, the label likelihood decomposes into a product over its tokens. We therefore aggregate token log-likelihoods and divide by $T(c)$ to obtain a per-token (length-normalized) score, ensuring labels with more tokens are not unfairly penalized.

To mitigate prior bias (i.e., the tendency to overestimate very frequent labels), we also compute a report-free NLL using only the prefix context:

$$\mathcal{L}_{\text{prior}}(c) = \frac{1}{T(c)} \sum_{t=1}^{T(c)} \left[-\log p_{\theta}(y_t | \text{prefix}, y_{<t}) \right].$$

This term captures how intrinsically common a label is under the model (with identical decoding setup), on the same per-token scale.

Finally, we combine the two losses into a PMI-style score by subtracting the report-free (prior) term from the report-conditioned term, with a nonnegative weight (α):

$$S(x, c) = -\mathcal{L}_{\text{cond}}(x, c) + \alpha \mathcal{L}_{\text{prior}}(c), \alpha \geq 0$$

Candidates are then sorted in descending order of $(S(x, c))$, and the top-(k) labels are returned as predictions. This construction explicitly removes the model’s unconditional tendency to emit high-frequency labels while keeping the two likelihoods comparable because they share the same prompt, tokenization, and length normalization. In all experiments we set ($\alpha = 1$), which offers a good trade-off: ($\alpha = 0$) collapses to pure conditional likelihood (and thus reintroduces frequency bias), whereas ($\alpha > 1$) can over-penalize labels that are common but still correct.

4. Results

4.1. GenMap (M1) vs. LL-Rank (M2)

We compare two prediction methods (GenMap and LL-Rank), and present the results in Table 1. Across seven backbones, the LL-Rank (M2) method consistently outperforms the GenMap (M1) baseline on nearly all metrics. Averaged over models, M2 increases Hit@3,5,10 by 80.1%, 85.7%, and 92.8%, and boosts Macro-F1@3,5,10 by 138.0%, 146.6%, and 156.7%, respectively. The gains are especially pronounced for Macro-F1, indicating that M2 strengthens performance on underrepresented labels rather than merely amplifying head classes. Improvements also grow from Top-3 through Top-10, suggesting that M2 not only raises the likelihood of retrieving a correct label early, but also produces a higher-quality ranked list overall.

4.2. Effect of the PMI Coefficient

Figure 1 examines how the LL-Rank method behaves as the PMI prior weight α varies. LL-Rank’s perfor-

Table 1: Comparison of two scoring methods. For each model we show M1 (GenMap), M2 (LL-Rank), and the relative improvement $\Delta = \frac{M2 - M1}{M1}$. $\bar{\Delta}$ is the mean percentage improvement across all models.

Model	Scoring	Top-3		Top-5		Top-10	
		Hit@3	Macro-F1	Hit@5	Macro-F1	Hit@10	Macro-F1
MedAlpaca (7B)	M1: GenMap	29.52	16.00	34.02	14.67	40.42	11.91
	M2: LL-Rank	67.99	35.86	76.92	31.02	84.53	23.81
	Δ	130.3%	124.1%	126.1%	111.5%	109.1%	99.9%
MedLLaMA (8B)	M1: GenMap	26.99	14.18	32.74	14.28	43.61	13.35
	M2: LL-Rank	49.89	28.43	61.30	24.45	75.68	16.48
	Δ	84.8%	100.5%	87.2%	71.2%	73.5%	23.4%
MedGEMMA (3B)	M1: GenMap	46.25	26.11	49.13	22.74	53.68	16.31
	M2: LL-Rank	42.57	26.74	52.13	23.88	65.39	20.02
	Δ	-8.0%	2.4%	6.1%	5.0%	21.8%	22.7%
AlphaMed (3B)	M1: GenMap	10.02	3.85	17.29	4.57	25.17	4.11
	M2: LL-Rank	20.27	17.75	32.05	24.08	58.67	27.46
	Δ	102.3%	361.0%	85.4%	426.9%	133.1%	568.1%
AlphaMed (7B)	M1: GenMap	30.32	15.92	36.42	15.66	44.72	12.92
	M2: LL-Rank	53.41	32.56	65.67	31.04	80.08	24.27
	Δ	76.2%	104.5%	80.3%	98.2%	79.1%	87.8%
MedFound (7B)	M1: GenMap	20.45	9.24	24.01	8.39	29.61	7.07
	M2: LL-Rank	32.84	20.15	41.86	20.92	56.75	20.31
	Δ	60.6%	118.1%	74.3%	149.3%	91.7%	187.3%
MedFound (8B)	M1: GenMap	18.94	11.27	22.69	11.05	30.87	10.53
	M2: LL-Rank	40.57	28.81	54.63	29.20	74.56	21.83
	Δ	114.2%	155.6%	140.8%	164.3%	141.5%	107.3%
$\bar{\Delta}$		80.1%	138.0%	85.7%	146.6%	92.8%	156.7%

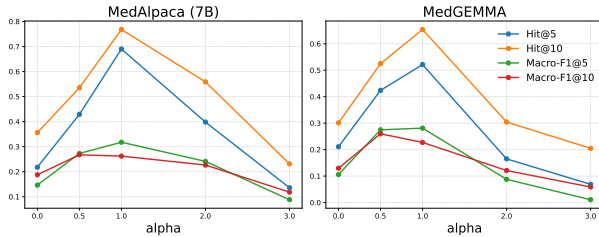


Figure 1: Effect of the PMI coefficient (α) on LL-Rank scoring.

mance is highly sensitive to the prior weight α . Across both backbones (MedAlpaca-7B and MedGEMMA-3B) performance peaks near $\alpha \approx 1$: when α is smaller, the prior under-corrects head-class bias and conditional likelihood dominates, leaving rare labels undervalued; when α is larger, the prior is over-applied, penalizing frequent labels too strongly and degrading the ranked list. The region around $\alpha \approx 1$ consistently

yields the best Hit and Macro F1. Compared with GenMap’s token-rarity heuristic, injecting an explicit prior via LL-Rank is markedly more effective for the long tail. Relative to no prior ($\alpha = 0$), setting $\alpha = 1$ roughly doubles performance on hit rate and macro F1.

5. Conclusion

We release MIMIC-SR-ICD11, a large English diagnostic dataset built from patient-authored self-reports and natively aligned with WHO ICD-11. On this resource, we instantiate LL-Rank, a likelihood-based re-ranking method that combines the conditional per-token likelihood of each label given the report with an explicit corpus-derived prior, counteracting head-class bias. Across seven backbones, LL-Rank consistently outperforms GenMap.

References

Zaid Al-Ars, Obinna Agba, Zhuoran Guo, Christiaan Boerkamp, Ziyaad Jaber, and Tareq Jaber. Nlice: Synthetic medical record generation for effective primary healthcare differential diagnosis. In *2023 IEEE 23rd International Conference on Bioinformatics and Bioengineering (BIBE)*, pages 397–402. IEEE, 2023.

Xuanzhong Chen, Xiaohao Mao, Qihan Guo, Lun Wang, Shuyang Zhang, and Ting Chen. Rarebench: can llms serve as rare diseases specialists? In *Proceedings of the 30th ACM SIGKDD conference on knowledge discovery and data mining*, pages 4850–4861, 2024.

Abhimanyu Dubey, Abhinav Jauhri, Abhinav Pandey, Abhishek Kadian, Ahmad Al-Dahle, Aiesha Letman, Akhil Mathur, Alan Schelten, Amy Yang, Angela Fan, et al. The llama 3 herd of models. *arXiv e-prints*, pages arXiv–2407, 2024.

Arsene Fansi Tchango, Rishab Goel, Zhi Wen, Julien Martel, and Joumana Ghosn. Ddxplus: A new dataset for automatic medical diagnosis. *Advances in neural information processing systems*, 35:31306–31318, 2022.

Tianyu Han, Lisa C Adams, Jens-Michalis Papaioannou, Paul Grundmann, Tom Oberhauser, Alexander Löser, Daniel Truhn, and Keno K Bressem. Medalpaca—an open-source collection of medical conversational ai models and training data. *arXiv preprint arXiv:2304.08247*, 2023.

Ruihui Hou, Shencheng Chen, Yongqi Fan, Lifeng Zhu, Jing Sun, Jingping Liu, and Tong Ruan. Msdiagnosis: An emr-based dataset for clinical multi-step diagnosis. *arXiv e-prints*, pages arXiv–2408, 2024.

Mingyi Jia, Junwen Duan, Yan Song, and Jianxin Wang. medIKAL: Integrating knowledge graphs as assistants of LLMs for enhanced clinical diagnosis on EMRs. In Owen Rambow, Leo Wanner, Marianna Apidianaki, Hend Al-Khalifa, Barbara Di Eugenio, and Steven Schockaert, editors, *Proceedings of the 31st International Conference on Computational Linguistics*, pages 9278–9298, Abu Dhabi, UAE, January 2025. Association for Computational Linguistics. URL <https://aclanthology.org/2025.coling-main.624/>.

Di Jin, Eileen Pan, Nassim Oufattolle, Wei-Hung Weng, Hanyi Fang, and Peter Szolovits. What disease does this patient have? a large-scale open domain question answering dataset from medical exams. *arXiv preprint arXiv:2009.13081*, 2020.

Qiao Jin, Bhuwan Dhingra, Zhengping Liu, William W. Cohen, and Xinghua Lu. Pubmedqa: A dataset for biomedical research question answering. In *Proceedings of the 2019 Conference on Empirical Methods in Natural Language Processing and the 9th International Joint Conference on Natural Language Processing (EMNLP-IJCNLP)*, pages 2567–2577, 2019.

Alistair E. W. Johnson, Tom J. Pollard, and Roger G. Mark. MIMIC-IV-Note: Deidentified free-text clinical notes (version 2.2), 2022. URL <https://doi.org/10.13026/1cjn-2370>.

Alistair E. W. Johnson, Lucas Bulgarelli, Tom Pollard, Brian Gow, Benjamin Moody, Steven Horng, Leo Anthony Celi, and Roger G. Mark. MIMIC-IV (version 3.1), 2024. URL <https://physionet.org/content/mimiciv/3.1/>. Accessed: 2025-05-13.

Che Liu, Haozhe Wang, Jiazen Pan, Zhongwei Wan, Yong Dai, Fangzhen Lin, Wenjia Bai, Daniel Rueckert, and Rossella Arcucci. Beyond distillation: Pushing the limits of medical llm reasoning with minimalist rule-based rl. *arXiv preprint arXiv:2505.17952*, 2025a.

Xiaohong Liu, Hao Liu, Guoxing Yang, Zeyu Jiang, Shuguang Cui, Zhaoze Zhang, Huan Wang, Liyuan Tao, Yongchang Sun, Zhu Song, et al. A generalist medical language model for disease diagnosis assistance. *Nature medicine*, 31(3):932–942, 2025b.

Harsha Nori, Mayank Daswani, Christopher Kelly, Scott Lundberg, Marco Tulio Ribeiro, Marc Wilson, Xiaoxuan Liu, Vikmesh Sounderajah, Jonathan Carlson, Matthew P Lungren, et al. Sequential diagnosis with language models. *arXiv preprint arXiv:2506.22405*, 2025.

Ankit Pal, Logesh Kumar Umapathi, and Malaikanan Sankarasubbu. Medmcqa: A large-scale multi-subject multi-choice dataset for medical domain question answering. In Gerardo Flores, George H. Chen, Tom Pollard, Joyce C. Ho, and Tristan Naumann, editors, *Proceedings of the Conference on Health, Inference, and Learning (CHIL)*, volume 174 of *Proceedings of Machine Learning Research*, pages 248–260. PMLR, 2022.

Pengcheng Qiu, Chaoyi Wu, Xiaoman Zhang, Weixiong Lin, Haicheng Wang, Ya Zhang, Yanfeng Wang, and Weidi Xie. Towards building multilingual language model for medicine. *Nature Communications*, 15(1):8384, 2024.

Andrew Sellergren, Sahar Kazemzadeh, Tiam Jaroensri, Atilla Kiraly, Madeleine Traverse, Timo Kohlberger, Shawn Xu, Fayaz Jamil, Cían Hughes,

Charles Lau, et al. Medgemma technical report. *arXiv preprint arXiv:2507.05201*, 2025.

Karan Singhal, Shekoofeh Azizi, Tao Tu, S. Sara Mahdavi, Jason Wei, Hyung Won Chung, Nathan Scales, Ajay Tanwani, Heather Cole-Lewis, Stephen Pfohl, Perry Payne, Martin Seneviratne, Paul Gamble, Chris Kelly, Abubakr Babiker, Nathanael Schärli, Aakanksha Chowdhery, Philip Mansfield, Dina Demner-Fushman, Blaise Agüera y Arcas, Dale Webster, Greg S. Corrado, Yossi Matias, Katherine Chou, Juraj Gottweis, Nenad Tomasev, Yun Liu, Alvin Rajkomar, Joelle Barral, Christopher Semturs, Alan Karthikesalingam, and Vivek Natarajan. Large language models encode clinical knowledge. *Nature*, 620(7972):172–180, 2023. doi: 10.1038/s41586-023-06291-2. URL <https://doi.org/10.1038/s41586-023-06291-2>. Published 2023/08/01.

Karan Singhal, Tao Tu, Juraj Gottweis, Rory Sayres, Ellery Wulczyn, Mohamed Amin, Le Hou, Kevin Clark, Stephen R. Pfohl, Heather Cole-Lewis, Darlene Neal, Qazi Mamunur Rashid, Mike Schaekermann, Amy Wang, Dev Dash, Jonathan H. Chen, Nigam H. Shah, Sami Lachgar, Philip Andrew Mansfield, Sushant Prakash, Bradley Green, Ewa Dominowska, Blaise Agüera y Arcas, Nenad Tomašev, Yun Liu, Renee Wong, Christopher Semturs, S. Sara Mahdavi, Joelle K. Barral, Dale R. Webster, Greg S. Corrado, Yossi Matias, Shekoofeh Azizi, Alan Karthikesalingam, and Vivek Natarajan. Toward expert-level medical question answering with large language models. *Nature Medicine*, 31(3):943–950, 2025. doi: 10.1038/s41591-024-03423-7. URL <https://doi.org/10.1038/s41591-024-03423-7>. Published 2025/03/01.

Zhixiang Su, Yinan Zhang, Jiazheng Jing, Jie Xiao, and Zhiqi Shen. Enabling patient-side disease prediction via the integration of patient narratives. In *Companion Proceedings of the ACM Web Conference 2024*, WWW ’24, page 581–584, New York, NY, USA, 2024. Association for Computing Machinery. ISBN 9798400701726. doi: 10.1145/3589335.3651498. URL <https://doi.org/10.1145/3589335.3651498>.

Gemma Team, Aishwarya Kamath, Johan Ferret, Shreya Pathak, Nino Vieillard, Ramona Merhej, Sarah Perrin, Tatiana Matejovicova, Alexandre Ramé, Morgane Rivière, et al. Gemma 3 technical report. *arXiv preprint arXiv:2503.19786*, 2025.

Qwen Team. Qwen2 technical report. *arXiv preprint arXiv:2407.10671*, 2024.

Hugo Touvron, Thibaut Lavril, Gautier Izacard, Xavier Martinet, Marie-Anne Lachaux, Timothée Lacroix, Baptiste Rozière, Naman Goyal, Eric Hambro, Faisal Azhar, et al. Llama: Open and efficient foundation language models. *arXiv preprint arXiv:2302.13971*, 2023.

Zhongyu Wei, Qianlong Liu, Baolin Peng, Huaixiao Tou, Ting Chen, Xuanjing Huang, Kam-fai Wong, and Xiangying Dai. Task-oriented dialogue system for automatic diagnosis. In Iryna Gurevych and Yusuke Miyao, editors, *Proceedings of the 56th Annual Meeting of the Association for Computational Linguistics (Volume 2: Short Papers)*, pages 201–207, Melbourne, Australia, July 2018. Association for Computational Linguistics. doi: 10.18653/v1/P18-2033. URL <https://aclanthology.org/P18-2033/>.

BigScience Workshop, Teven Le Scao, Angela Fan, Christopher Akiki, Ellie Pavlick, Suzana Ilić, Daniel Hesslow, Roman Castagné, Alexandra Sasha Lucioni, François Yvon, et al. Bloom: A 176b-parameter open-access multilingual language model. *arXiv preprint arXiv:2211.05100*, 2022.

Lin Xu, Qixian Zhou, Ke Gong, Xiaodan Liang, Jianheng Tang, and Liang Lin. End-to-end knowledge-routed relational dialogue system for automatic diagnosis. In *Proceedings of the AAAI conference on artificial intelligence*, volume 33, pages 7346–7353, 2019.

Xiaohua Zhai, Basil Mustafa, Alexander Kolesnikov, and Lucas Beyer. Sigmoid loss for language image pre-training. In *ICCV*, 2023. URL <https://arxiv.org/abs/2303.15343>.

Shuang Zhou, Mingquan Lin, Sirui Ding, Jiashuo Wang, Canyu Chen, Genevieve B Melton, James Zou, and Rui Zhang. Explainable differential diagnosis with dual-inference large language models. *npj Health Systems*, 2(1):12, 2025.

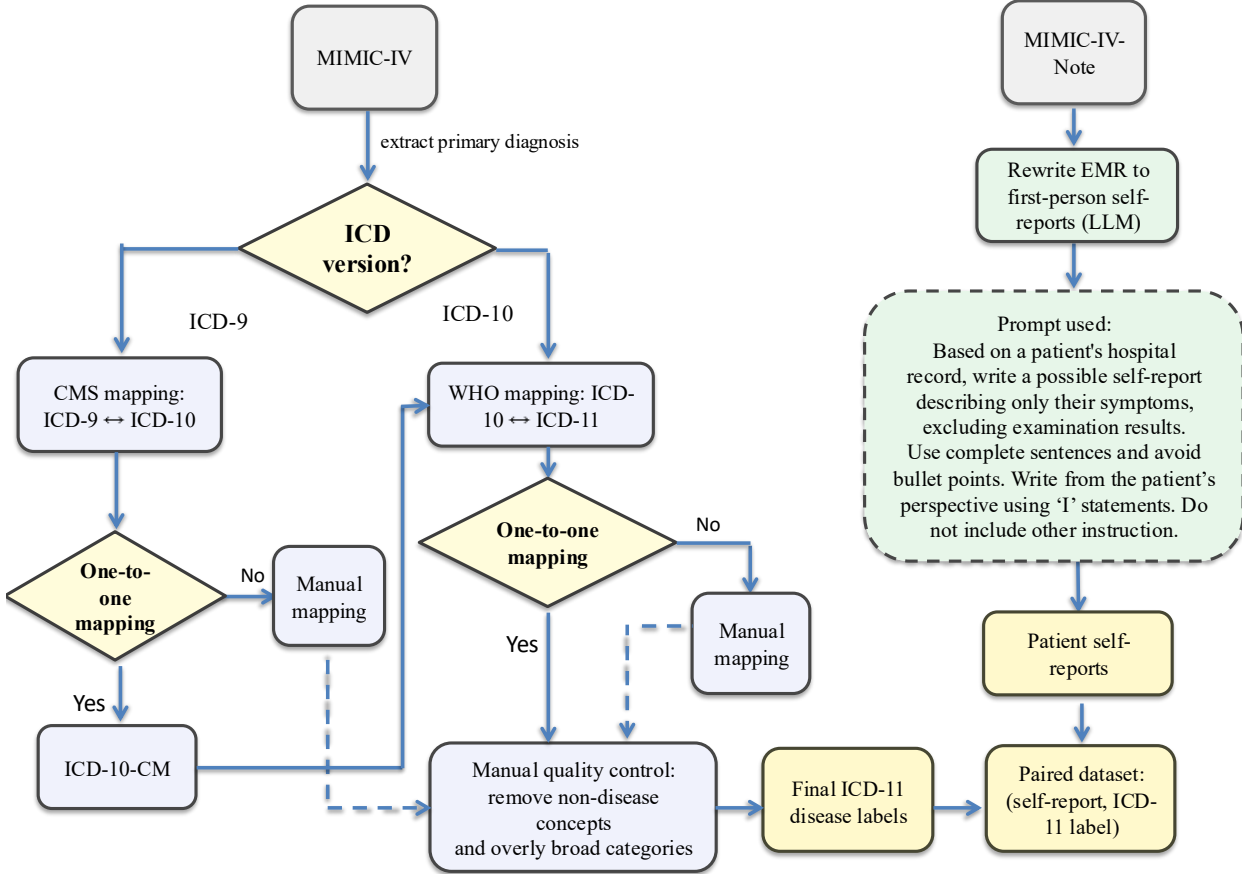


Figure 2: Data construction pipeline. Left branch: extract primary diagnoses from MIMIC-IV and map ICD-9 to ICD-10 then ICD-10 to ICD-11, with one-to-one filtering and manual quality control. Right branch: rewrite MIMIC-IV-Note into first-person self-reports using ChatGPT. The dashed box shows the exact prompt we used in practice. Outputs: final ICD-11 labels and paired records.

Appendix A. Dataset Construction and Preprocessing

Figure 2.

Appendix B. Related Work

In this section we review recent diagnosis-oriented datasets. We organize the landscape into two streams: (i) symptom-inquiry policy learning, which focuses on interactive, slot-based symptom collection, and (ii) full-text diagnostic inference, which infers diseases from unstructured narratives. Table 2 summarizes key properties (e.g. scale, disease coverage, real world provenance, support for patient self-reports (SR), free-

text availability, ontology alignment, language) and contrasts them with our proposed MIMIC-SR-ICD11.

Symptom-inquiry policy learning Symptom-inquiry policy learning views the clinical interview as sequential evidence gathering: the system chooses which symptom to ask about next until it has enough information to issue a diagnosis. Representative datasets for this scenario include Muzhi Wei et al. (2018), DX, DDXPlus Fansi Tchang et al. (2022), NLICE Al-Ars et al. (2023), RareBench Chen et al. (2024), SDBench Nori et al. (2025), and Open-XDDx Zhou et al. (2025). Muzhi introduces small task-oriented diagnostic dialogues centered on follow-up symptom questioning. DX builds on this by moving from curated toy dialogues to real-world online con-

Table 2: Comparison of diagnosis datasets. Columns: Dis.# = number of disease categories; Real = real-world provenance; Gen. = generalist coverage; SR = patient self-report; Free-text = unstructured input; Ont = ontology alignment (e.g., ICD-11); Lang = language.

Dataset / Benchmark	Size	Dis.#	Real	Gen.	SR	Free-text	Ont	Lang
Muzhi Wei et al. (2018)	710	4	✗	✗	✓	✓	✗	ZH
DX Xu et al. (2019)	527	5	✓	✗	✓	✓	✗	ZH
DDXPlus Fansi Tchang et al. (2022)	1,300,000	49	✗	✗	✗	✗	✗	EN
NLICE Al-Ars et al. (2023)	1,000,000	55	✗	✗	✗	✗	✗	EN
RareBench Chen et al. (2024)	2,185	421	✓	✗	✗	✓	✓	ZH/EN
MSDiagnosis Hou et al. (2024)	2,225	—	✓	✓	✗	✓	✗	ZH
Haodf Su et al. (2024)	29,326	190	✓	✓	✓	✓	✗	ZH
SDBench Nori et al. (2025)	304	—	✓	✓	✗	✓	✗	EN
Open-XDDx Zhou et al. (2025)	570	—	✗	✓	✗	✓	✗	EN
CMEMR Jia et al. (2025)	10,450	—	✓	✓	✗	✓	✗	ZH
MIMIC-SR-ICD11 (Ours)	119,178	118	✓	✓	✓	✓	✓	EN

sultations with free-text narratives. RareBench shifts the focus to rare diseases and standardizes labels via clinical ontologies, enabling standardized evaluation. SDBench then changes the mode from static dialogue to a step-by-step case: at each step the system can ask more history or order a test, and every test has a price tag—the aim is to reach the correct diagnosis while spending as little as possible. Open-XDDx keeps the narrative format and adds expert rationales, allowing assessment of both accuracy and the quality of explanations. Because these practice-derived resources are small (hundreds to a few thousand cases), they are best suited for prompting, few-shot evaluation, or lightweight instruction/preference tuning—often with synthetic augmentation—rather than stable supervised fine-tuning of billion-parameter LLMs. To address scale, synthetic cohorts such as DDXPlus and NLICE expand to hundreds of thousands or millions of encounters and enrich symptoms from binary indicators to multi-dimensional descriptors (e.g., location, intensity, duration), improving controllability and reproducibility while remaining compatible with sequential decision formulations; however, by omitting free-text self-reports they sacrifice realism, which can hinder direct transfer to narrative-driven diagnostic workflows.

Full-text Diagnostic Inference Unlike resources built for symptom-inquiry policy learning, full-text diagnostic inference (FTDI) evaluates models on complete clinical narratives: the system reads an entire note or consultation and then predicts the diagnosis. Datasets in this setting include MSDiagnosis [Hou et al. \(2024\)](#), Haodf [Su et al. \(2024\)](#), and CMEMR [Jia et al. \(2025\)](#). MSDiagnosis and CMEMR are Chinese EMR

corpora for document-level diagnosis. In both, gold diagnoses are free text. Compared with MSDiagnosis (2.2k cases across 12 departments), CMEMR scales to 10.5k cases with broader specialty coverage and richer, longer documents—including admission notes, hospital course, and lab/imaging summaries—making it well suited for long-form diagnostic inference and information extraction. In contrast to these clinician-authored EMRs, Haodf is patient-side: it collects real online consultations with free-text self-reports and physician replies, covering many common conditions. It is valuable for generalist triage/diagnosis from the patient’s perspective. However, labels are not natively ontology aligned and the corpus is Chinese only, which complicates cross-dataset comparison and large-scale finetuning.

In summary, datasets for symptom-inquiry policy learning are mostly small, practice-derived free-text corpora. By contrast, DDXPlus and NLICE scale to hundreds of thousands or millions of cases but drop free text, limiting realism. Existing full-text diagnostic inference (FTDI) corpora are predominantly Chinese (e.g., MSDiagnosis, CMEMR, Haodf). Most resources above also lack native ontology alignment. Their labels are free-named and mapped to a standard vocabulary only at evaluation time. Compared with these datasets, our proposed MIMIC-SR-ICD11 is, to our knowledge, the first large-scale, English, patient self-report dataset for FTDI with native ICD-11 standardization. This design reduces linguistic ambiguity, removes fragile post-hoc mapping during evaluation, and offers generalist coverage (118 diagnoses) at benchmark scale (119k reports). We release fixed splits and

Table 3: Summary of baseline models.

Model(s)	Size	Method	Objective	Data Source	Backbone
MedAlpaca	7B	SFT	QA / dialogue	med education	LLaMA v1
MMedLLaMA	8B	DAPT + SFT	MCQ (with rationales)	med knowledge, med education	Llama 3
MedGEMMA	3B	VLP + SFT + RL	VLM QA / report generation	med education	Gemma-3
AlphaMed	3B / 7B	RL (GRPO)	MCQ (boxed final)	med education	Qwen2 / Qwen2.5
MedFound	7B / 8B	DAPT + Cot + DPO	Diagnostic reasoning	clinical notes, med reference	BLOOM / Llama 3

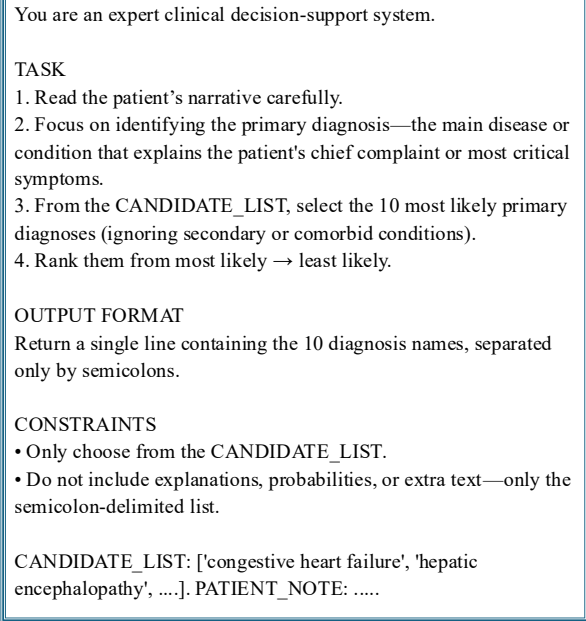


Figure 3: Illustration of the standardized prompt format (instruction, candidate list, and patient self-report) provided to the general LLMs.

an evaluation script to enable reproducible training and fair comparison.

Appendix C. Experiments

C.1. Baseline

C.1.1. MEDICAL DOMAIN LLMs

MedAlpaca [Han et al. \(2023\)](#): An instruction-tuned family built on LLaMA backbones (7B and 13B) [Touvron et al. \(2023\)](#), trained on 160k medical instruction pairs reformatted into Q/A and chat style. The corpus blends medical-education questions, community Q&A, and wiki-style textbook/patient-information prose, yielding conversational prompts and short rationales suitable for clinical knowledge querying.

MMedLlama [Qiu et al. \(2024\)](#): An 8B Llama 3 [Dubey et al. \(2024\)](#) medical model obtained by continued auto-regressive domain adaptation on a 25.5B-token multilingual medical corpus (six languages), followed by supervised fine-tuning on multilingual multiple-choice medical QA with rationales. The pre-training data are knowledge-oriented medical texts, rather than patient–doctor dialogues. The supervised stage targets medical-education style Q&A across broad specialties.

MedGEMMA [Sellergren et al. \(2025\)](#): A multimodal medical LLM built on the Gemma-3 [Team et al. \(2025\)](#) architecture with a SigLIP-400M vision encoder [Zhai et al. \(2023\)](#) and long-context image–text interleaving. Its training proceeds in three stages: (1) vision-encoder enhancement on medical image–text pairs (covering radiology, dermatology, histopathology, and ophthalmology, including 32.6M histopathology patches); (2) multimodal decoder pretraining that mixes medical image-text data with the original general-domain mixture to preserve general VLM capabilities; and (3) post-training that adds medical instruction data via distillation and uses reinforcement learning with paired medical image–text to surface multimodal skills.

AlphaMed [Liu et al. \(2025a\)](#): A medical LLM built on a Qwen-family [Team \(2024\)](#) backbone and trained purely with rule-based reinforcement learning (GRPO), with no supervised fine-tuning or distilled chain-of-thought. The training set comprises 400k multiple-choice medical QA items. These are medical-education–style multiple-choice questions intended for exam-like diagnostic reasoning rather than patient–doctor dialogues.

MedFound [Liu et al. \(2025b\)](#): A generalist medical LLM with 7B and 176B parameter variants built on a BLOOM-family [Workshop et al. \(2022\)](#), decoder-only Transformer backbone. It is pretrained on large-scale medical text and de-identified real-world clinical records, then adapted for diagnostic reasoning via a self-bootstrapping chain-of-thought phase and a preference-alignment step (DPO) to better match clinician practice. The training emphasizes long-form

You are a clinical writing evaluator. Use ONLY the persona and the PATIENT-STATED EHR excerpt as ground truth. Evaluate the candidate self-report strictly against that.

Inputs

- Persona (JSON): {persona_json}
- EHR (patient-stated only): {ehr_text}
- Candidate self-report: {candidate_report}

Scores (1–5) & weights

- ClinicalCorrectness (0.40): Score only the claims actually made in the report (affirmed symptoms or explicit denials).
- Zero-claim rule: if the report makes NO symptom claims at all, set ClinicalCorrectness = 5.0.
- Semantic match: count synonyms/abbreviations/paraphrases if they clearly refer to the same symptom TODAY (e.g., SOB ↔ shortness of breath; loose stools ↔ diarrhea; can't keep food down ↔ vomiting).
- Negation scope & timing: a denial is supported only if TODAY'S EHR states the same denial.
- Contradictions: if the report asserts the opposite of TODAY'S EHR, penalize heavily.
- Unsupported new facts: penalize new medical facts not in the EHR; do NOT penalize neutral paraphrases.
- Omissions: do NOT penalize omissions unless they create a contradiction.
- Faithfulness (0.30): Only patient-stated facts; no leakage of exam, vitals interpretation, labs/imaging, inpatient course, diagnoses, or treatment speculation.
- Persona (0.20): Tone/word choice align with persona cues (education, age, language, setting) without adding facts.
- Realism (0.10): Natural first-person voice; concise; selective denials (not exhaustive lists); plausible length/cadence for the setting/persona.

$$\text{overall} = 0.30 \cdot \text{Faithfulness} + 0.40 \cdot \text{ClinicalCorrectness} + 0.20 \cdot \text{Persona} + 0.10 \cdot \text{Realism}$$

Output (JSON only)

```
{
  "Faithfulness": <1-5>,
  "ClinicalCorrectness": <1-5>,
  "Persona": <1-5>,
  "Realism": <1-5>,
  "overall": <1-5>
}
```

Figure 4: Prompt used for evaluation.

clinical narratives and physician-style inference rather than short factoid QA.

C.1.2. GENERAL LLMs

Table 5: General LLM baselines used in our study. Prices are public API list rates *per 1M tokens*, shown as *input / output*

Model	Release date	Price
Gemini 2.5 Flash	2025-06-17	\$0.30 / \$2.50
Claude 4 Sonnet	2025-05-22	\$3.00 / \$15.00
ChatGPT (o3)	2025-04-16	\$2.00 / \$8.00
ChatGPT (GPT-5)	2025-08-07	\$1.25 / \$10.00

We conduct our experiments on four latest LLMs: (1) Gemini 2.5 Flash (Google): a fast, low-cost mul-

timodal model optimized for high-throughput extraction/summarization and long-context use; (2) Claude 4 Sonnet (Anthropic): a balanced, enterprise-oriented model with reliable long-context reasoning, strong structure-following, and safety; (3) ChatGPT (o3)(OpenAI): a reasoning-first model that allocates extra compute to step-by-step problem solving and integrates tightly with function calling; (4) ChatGPT (GPT-5) (OpenAI): a next-generation flagship emphasizing improved planning and agentic behavior alongside stronger coding and tool orchestration.

C.2. Evaluation of Dataset Quality

LLM-Based Evaluation To assess the intrinsic quality of our dataset (rather than model capability), we uniformly sample 10000 report–EHR pairs from

Table 4: Summary of linguistic metrics. (Avg) Length: mean tokens, sentences, and tokens/sentence. Lexical diversity (LexDiv) = unique word types \div total tokens; FK (Flesch–Kincaid) grade estimates the U.S. school grade level needed to read the text, higher is harder. POS / Content (%): share of content words (ADJ+ADV+VERB+NOUN) and each POS.

Generator	(Avg) Length	Lexicon & Readability			POS / Content (%)				
	tokens sents sent len	Vocab	LexDiv%	FK	Content	Adj	Adv	Verb	Noun
Origin	153.45 7.22 21.70	101.97	68.06	12.89	51.70	10.17	4.45	13.35	23.73

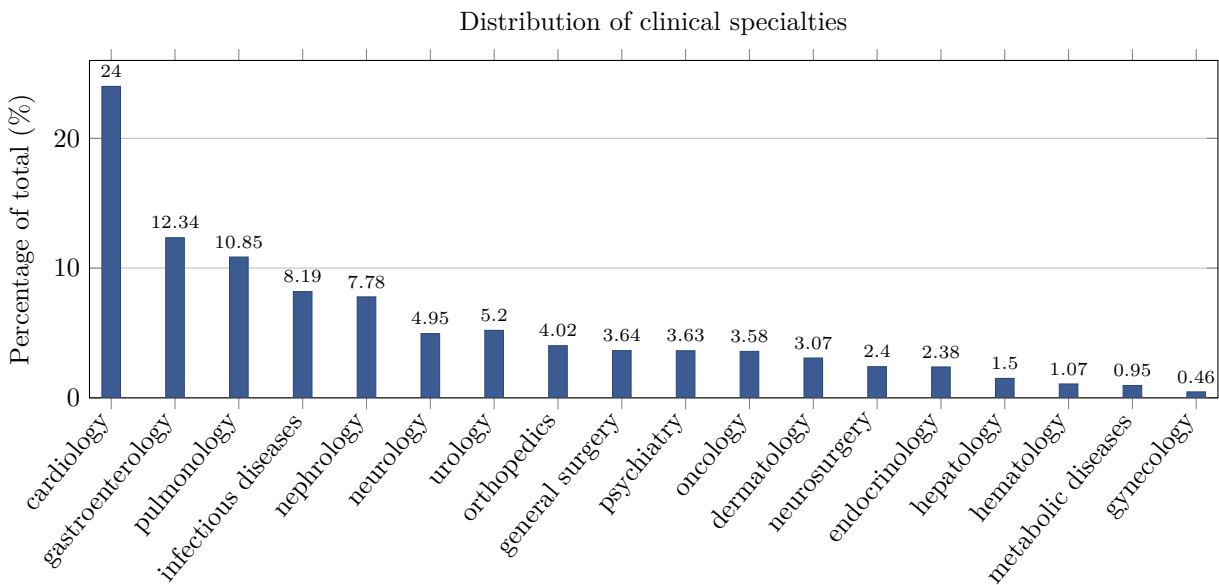


Figure 5: Distribution of clinical specialties in the primary-diagnosis subset.

the corpus and evaluate each case with the prompt in Fig. 4. The prompt captures both clinical fidelity and patient-style quality along four dimensions: clinical correctness, faithfulness, persona alignment, and realism. We prioritize Clinical Correctness and faithfulness in the overall score, assigning weights of 0.40 and 0.30; Persona alignment and Realism carry secondary weights of 0.20 and 0.10.

For clinical Correctness, we score only claims explicitly made in the self-report and compare them against the patient-stated EHR excerpt; omissions do not incur penalties, whereas contradictions and unsupported medical facts do. For faithfulness, we require that all content originate from the patient-stated EHR and explicitly exclude clinician interpretations, examinations or test results, diagnoses, and treatment speculation. persona alignment and realism evaluate the naturalness and plausibility of the narrative, cap-

turing whether language, tone, and structure match how a real patient would describe symptoms.

Two independent LLM graders (GPT-4.1 and Claude Sonnet 3.7) apply the same rubric to every case, yielding comparable scores for cross-grader validation and fairness analysis. This framework standardizes evaluation, reduces subjective bias, and keeps the assessment focused on how accurately and authentically the reports reflect patient-stated content.

Cross-Dataset Consistency Evaluation To further assess dataset quality, we test whether models trained on the self-report corpus exhibit consistent behavior on the original EHR data. Each model is first fine-tuned on the self-report dataset and evaluated on both self-report and EHR test sets (before-tune). We then perform an additional fine-tuning step on a 5K-sample, label-balanced EHR subset after-tune and re-evaluate on both domains.

Table 6: Comparison of two graders—GPT-5 and Claude Sonnet 3.7—on three generators (Origin=no-persona baseline, GPT-4o-mini, GPT-5-mini). Cells show mean \pm SD for *Clinical Correctness*, *Faithfulness*, *Persona*, *Realism*, and *Overall* (higher is better). The last two rows report MAE $|\text{diff}|$ and tolerance $P(|\text{diff}| \leq 0.50)$.

Generator	Grader	Clinical Correctness	Faithfulness	Persona	Realism	Overall
Origin	GPT-4.1	4.23 ± 1.14	4.38 ± 0.80	4.76 ± 0.26	4.56 ± 0.31	4.39 ± 0.60
	Sonnet 3.7	4.25 ± 1.08	4.21 ± 1.21	4.01 ± 0.35	4.08 ± 0.32	4.17 ± 0.71
	$ \text{diff} $	0.359	0.375	0.765	0.615	0.370
	$P(\text{diff} \leq 0.50)$	0.769	0.808	0.473	0.631	0.799

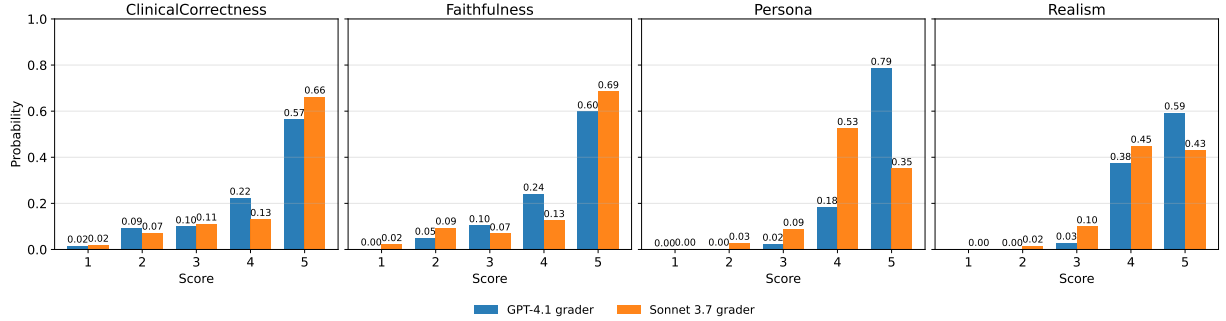


Figure 6: Probability mass functions (PMFs) of the 1–5 rating scores for *Clinical Correctness*, *Faithfulness*, *Persona*, and *Realism*. GPT-4.1 and Sonnet 3.7 score the same set of GPT-4o *no-persona* self-reports. Scores in [1, 5] are binned at $\{0.5, 1.5, 2.5, 3.5, 4.5, 5.5\}$ and normalized to 1.

If the self-report and EHR datasets are distributionally consistent, post-fine-tuning improvements on EHR should not substantially reduce performance on self-report data. This comparison measures cross-dataset alignment: smaller performance divergence after EHR fine-tuning indicates higher dataset fidelity and generalization stability.

C.3. Experiment Setting

We fine-tune the model for three epochs with batch size of 16. The optimizer uses a cosine learning-rate schedule with an initial learning rate of 1×10^{-4} and a warm-up of 50 steps. During training, we clip gradients to a maximum global norm of 1.0 and use bfloat16 precision. We adopt LoRA for parameter-efficient fine-tuning (rank 16, scaling 32, dropout 0.05, no bias), attaching adapters to all attention projections and to the feed-forward block. To evaluate general-purpose LLMs, we use the prompt shown in Fig. 3.

Appendix D. Data

D.1. Data Statistics

To quantify the linguistic and clinical coverage of the dataset, we summarize its key properties in two complementary views.

Table 4 presents the linguistic statistics of the original self-reports. The texts are concise on average (153 tokens per report, 7 sentences per case), yet linguistically diverse with a lexical diversity of 68.06% and a Flesch–Kincaid grade level of 12.9, indicating natural but domain-rich patient language. The proportion of content words (51.7%) and balanced part-of-speech distribution further suggest that the generated narratives are information-dense while maintaining fluency and readability.

Figure 5 illustrates the distribution of clinical specialties in the primary-diagnosis subset. Cardiology, gastroenterology, and pulmonology are the most represented specialties, followed by infectious diseases and nephrology. Meanwhile, long-tail areas such as endocrinology, hematology, and metabolic disorders are also covered, ensuring that both high-frequency and rare conditions are included. This balanced coverage supports fair model evaluation across diverse disease categories.

Table 7: We evaluate whether our generated self-report dataset is distributionally consistent with the original EHR dataset. Each model is first trained on the self-report dataset, then further fine-tuned on a 5K-sample EHR subset. We compare performance on both EHR and self-report before and after the EHR fine-tuning. If the two datasets have similar distributions, their post-fine-tuning performance should be close.

Model	Phase	EHR			self-report		
		hit@3	hit@5	hit@10	hit@3	hit@5	hit@10
medalpha	before-tune	0.7413	0.8433	0.9220	0.6873	0.7953	0.9007
	after-tune	0.7727	0.8720	0.9260	0.7053	0.8167	0.9033
	improvement	+4.2%	+3.4%	+0.4%	+2.6%	+2.7%	+0.3%
medllama	before-tune	0.7407	0.8533	0.9380	0.6767	0.7873	0.8973
	after-tune	0.7660	0.8727	0.9433	0.6867	0.8000	0.8987
	improvement	+3.4%	+2.3%	+0.6%	+1.5%	+1.6%	+0.2%
alphamed(3b)	before-tune	0.3447	0.4620	0.6507	0.3833	0.5120	0.7200
	after-tune	0.4547	0.5600	0.7560	0.3820	0.5133	0.7200
	improvement	+31.9%	+21.2%	+16.2%	-0.3%	+0.3%	+0.0%
alphamed(7b)	before-tune	0.6113	0.7173	0.8400	0.6053	0.7127	0.8313
	after-tune	0.6707	0.7760	0.8860	0.6260	0.7353	0.8473
	improvement	+9.7%	+8.2%	+5.5%	+3.4%	+3.2%	+1.9%
medfound(7b)	before-tune	0.3807	0.4593	0.5787	0.3660	0.4427	0.5660
	after-tune	0.4907	0.5760	0.7387	0.4327	0.5340	0.6807
	improvement	+28.9%	+25.4%	+27.6%	+18.2%	+20.6%	+20.3%
medfound(8b)	before-tune	0.6393	0.7620	0.8860	0.5800	0.6973	0.8407
	after-tune	0.6467	0.7720	0.8893	0.5827	0.7120	0.8600
	improvement	+1.2%	+1.3%	+0.4%	+0.5%	+2.1%	+2.3%

Together, these statistics demonstrate that the dataset is linguistically coherent, clinically diverse, and suitable for evaluating diagnostic reasoning across a broad spectrum of medical specialties.

These results collectively indicate strong cross-grader reliability and justify the use of automatic LLM graders for large-scale quality assessment of synthetic self-reports.

D.2. LLM-based Dataset Quality Evaluation

Table 6 summarizes the mean \pm standard deviation of the four evaluation dimensions: *Clinical Correctness*, *Faithfulness*, *Persona*, and *Realism*, as well as the combined *Overall* score. Both models yield highly correlated ratings, with average disagreement below 0.4 and over 75% of cases within ± 0.5 , demonstrating that the rubric is reproducible and robust across different evaluators.

Figure 6 further visualizes the discrete score distributions for each metric. The probability mass functions (PMFs) show that GPT-4.1 and Sonnet 3.7 exhibit closely aligned patterns, though GPT-4.1 tends to assign slightly higher realism and persona scores.

D.3. Dataset Consistency Evaluation

Table 7 compares model performance before and after EHR fine-tuning, confirming that gains on EHR data transfer well to self-reports. We report only Hit@k metrics (Hit@3/5/10). F1 scores are intentionally omitted, as they are highly sensitive to per-label variability and class imbalance. Because the EHR fine-tuning subset is intentionally balanced, reporting F1 would conflate true distributional consistency with the artificial balance of the training set. To avoid introducing bias from label imbalance, we therefore use Hit@k as a direct and distribution-agnostic indicator of dataset alignment.

Table 8: Results on a 1514 sample subset comparing general LLM APIs and medical-domain open models fine-tuned with SFT/LoRA. Bold indicates the best score in each column. The last line of each block (*Average*) gives the mean across models in that block, enabling a direct group-level comparison.

Model	Top-3		Top-5		Top-10	
	Hit@3	Macro-F1	Hit@5	Macro-F1	Hit@10	Macro-F1
<i>Zero-shot APIs (general models)</i>						
Gemini 2.5 Flash	55.02	23.79	64.86	20.26	74.50	15.00
Claude 4	60.36	26.58	72.26	19.46	83.29	14.33
ChatGPT (o3)	66.03	34.50	74.77	28.12	82.76	19.00
ChatGPT (GPT-5)	66.12	32.58	74.83	26.30	83.75	16.91
<i>Average</i>	61.88	29.36	71.68	23.54	81.08	16.31
<i>SFT/LoRA (medical models)</i>						
MedAlpaca (7B)	67.86	39.31	77.84	34.80	85.43	26.94
MMedLLaMA (8B)	69.26	39.11	80.24	33.81	89.35	24.54
MedGEMMA (3B)	48.84	33.66	58.88	32.25	70.99	25.47
AlphaMed (3B)	21.02	17.85	35.33	25.33	56.22	29.17
AlphaMed (7B)	54.29	34.22	66.60	33.36	79.91	26.46
MedFound (7B)	33.60	21.44	42.25	21.47	54.16	21.13
MedFound (8B)	57.62	38.50	70.53	37.43	85.63	27.91
<i>Average</i>	50.36	32.73	61.67	31.21	74.53	25.95

Table 9: Per-specialty average Top-5 hit rate across models. Abbreviations: MA = MedAlpaca, ML = MedLLaMA, MG = MedGEMMA, AM-3B = AlphaMed (3B), AM-7B = AlphaMed (7B), MF-7B = MedFound (7B), MF-8B = MedFound (8B).

Specialty	MA	ML	MG	AM-3B	AM-7B	MF-7B	MF-8B
Cardiology	75.5	58.9	23.4	26.6	64.9	41.9	59.6
Dermatology	73.0	36.1	0.2	47.5	92.5	27.0	55.6
Endocrinology	94.4	82.5	33.1	67.7	84.8	36.7	88.0
Urology	73.2	7.0	0.0	2.8	40.8	28.2	8.5
Gastroenterology	85.2	56.5	27.9	27.8	70.6	50.0	54.5
General Surgery	90.0	82.0	38.6	33.6	86.9	63.5	72.4
Gynaecology	100.0	100.0	74.0	98.0	98.0	96.0	100.0
Hematology	74.6	60.7	0.0	24.2	60.2	48.5	65.3
Hepatology	93.7	39.2	58.7	46.6	73.9	41.4	33.8
Infectious Diseases	67.2	40.3	22.0	17.7	43.4	27.9	18.2
Nephrology	45.7	53.3	10.6	14.9	41.4	38.7	47.9
Neurology	89.0	67.5	34.1	35.7	74.0	13.9	62.8
Neurosurgery	86.2	62.7	31.7	26.8	74.8	19.6	60.5
Metabolic Diseases	6.1	92.1	94.7	43.0	88.6	70.2	96.5
Oncology	88.8	43.1	21.3	30.2	53.0	34.2	56.3
Orthopaedics	94.2	91.4	84.5	51.1	61.4	69.2	85.7
Psychiatry	89.3	61.5	39.8	49.5	79.6	47.4	68.2
Pulmonology	59.4	69.2	25.7	42.6	61.1	54.5	63.5
Urology	86.8	76.7	65.0	60.6	82.4	53.9	66.8

Across all model families, EHR fine-tuning consistently improves diagnostic accuracy on the EHR test set, confirming effective domain adaptation. Importantly, these gains do not come at the cost of large performance drops on the self-report test set—Hit@k

scores on self-report data remain stable or even slightly improve (e.g., +2–3 pp for MedAlpaca and MedFound). This indicates that the synthetic self-reports share a closely aligned label and feature distribution with the original EHR notes. Smaller models such

as AlphaMed-3B show larger improvements (+31.9 % Hit@3 on EHR) due to their initial underfitting and stronger sensitivity to data augmentation, whereas larger backbones (e.g., MedFound-8B) exhibit only marginal gains, suggesting better cross-domain generalization even before EHR fine-tuning.

In conclusion, the alignment between self-report and EHR performance demonstrates that the proposed MIMIC-SR-ICD11 corpus captures medically faithful and distributionally consistent representations of the original clinical data. Fine-tuning on synthetic self-reports therefore transfers reliably to real EHR inputs, validating the dataset’s utility for scalable pretraining and model adaptation in clinical NLP.

Appendix E. Result

E.1. Comparison of General and Medical Models

General LLM APIs often have substantial usage cost (Table 5). For instance, running GPT-5 once over our 1514 samples cost more than \$40. To reduce cost while retaining accuracy, we fine-tune smaller open models for this task and compare them against general LLMs (shown in the table 8). The evaluation subset contains 1000 randomly sampled notes plus 514 supplementary notes chosen to ensure at least ten cases per label, so Macro-F1 is not unduly driven by very rare classes.

Across models, the largest gains from medical LLMs appear on Macro-F1—especially at Top-10, where the average improvement is nearly ten absolute points—indicating better coverage of underrepresented labels rather than mere boosts on head classes. This pattern is consistent with two effects of task-aligned fine-tuning: (i) exposure to domain terminology and label phrasing increases lexical fidelity to the ICD-11 space; and (ii) training on task distributions tempers over-confident, generic completions, yielding a more balanced precision–recall trade-off on the long tail. While general-purpose APIs deliver strong hit rates, several compact medical models (e.g., MMedL-LaMA (8B) and MedAlpaca (7B)) outperform the best general model (ChatGPT) on all columns. GPT-5 and the reasoning-optimized ChatGPT (o3) perform similarly, suggesting limited additional benefit from generic chain-of-thought without domain adaptation. Overall, careful fine-tuning of smaller medical models can match or exceed costlier general LLM APIs while being substantially cheaper to operate.

E.2. Per-Specialty and Per-Disease Hit@5

Table 9 and Table 10 summarize per-specialty and per-disease Hit@5 results, respectively. The results indicate that different models demonstrate heterogeneous learning capabilities across specialties and disease types, offering a reference for future studies on model generalization and domain-specific adaptation.

Appendix F. Application Scenarios

The proposed MIMIC-SR-ICD11 dataset and accompanying diagnostic framework can serve as a foundation for multiple downstream applications in clinical decision support. We highlight two representative use cases where patient-style self-reports and probabilistic diagnosis prediction can be directly integrated into hospital workflows.

(1) Triage Optimization. Within emergency or outpatient settings, the system can continuously monitor predicted diagnostic confidence scores. When the probability of a high-risk condition exceeds a predefined threshold, the model issues a *fast-track flag* to prioritize urgent evaluation. This mechanism enables early identification of critical cases, reduces waiting time for severe or rapidly progressing diseases, and supports optimal allocation of limited medical resources.

(2) Diagnostic Planning Assistance. For each incoming case, the model dynamically generates an *examination checklist trigger*, outlining key laboratory or imaging tests that would best distinguish among the top-ranked differential diagnoses. For instance, when multiple cardiopulmonary disorders are predicted with comparable confidence, the system may recommend targeted tests such as echocardiography or D-dimer assays to resolve diagnostic ambiguity. This functionality not only accelerates clinical decision-making but also contributes to cost-effective medical practice by minimizing unnecessary investigations.

Appendix G. License and Availability

We distribute our fine-tuned LoRA checkpoint under the *PhysioNet Credentialed Health Data License v1.5.0* (PHDDL v1.5.0)—the very same licence that governs the original MIMIC-IV corpus. In practical terms this entails:

1. **Who may download.** Access is restricted to researchers who: (i) have successfully com-

pleted CITI training; (ii) have signed the official MIMIC-IV data-use agreement; (iii) hold an active PhysioNet credential.

2. **Where to download.** The checkpoint is hosted *exclusively* inside the PhysioNet platform (project ID: `physionet-2026-xxx`). No copy is made available on public model hubs, cloud buckets, or version-control mirrors.
3. **How to redistribute.** Any further redistribution must preserve the *same* licence and the *same* access-control mechanism. Uploading the weights to public repositories (e.g. the Hugging Face Hub or an open Google Cloud bucket) is therefore not permitted.

All training scripts, inference code, and preprocessing utilities are released under the permissive **Apache-2.0** licence at <[anonymised-GitHub-URL](#)>. These scripts contain *no* portion of the original MIMIC text and may thus be freely reused.

Appendix H. Artifact Usage and Intended Use

H.1. Use of Existing Artifacts

We relied on several third-party resources, each with its own access and usage restrictions:

- MIMIC-IV and MIMIC-IV-Note are governed by PhysioNet’s credentialed access agreement, which permits use for non-commercial, research-only purposes. All analysis in this paper was conducted under that agreement and in compliance with its requirement that no clinical or commercial deployment occur.
- WHO ICD-11 API is provided under the WHO open data policy. We used it strictly to normalize diagnoses in our dataset, in accordance with the API’s terms for research and educational use.

In each case, our usage matches the intended research-only context and does not violate any access conditions or licensing terms.

H.2. Intended Use of Created Artifacts

We release the MIMIC-SR-ICD11 dataset (and accompanying code) under the Creative Commons Attribution 4.0 International (CC BY 4.0) license. This license permits unrestricted research and educational

reuse, provided that appropriate credit is given. In keeping with PhysioNet’s original agreement, we explicitly restrict MIMIC-SR-ICD11 to non-commercial, research-only applications. Users who wish to employ the dataset for clinical decision support or commercial purposes must first secure the necessary permissions from the data providers.

Appendix I. Ethics

All human-subject data in this study (MIMIC-IV and MIMIC-IV-Note) are fully de-identified under HIPAA and were released under a PhysioNet Data Use Agreement (DUA) that mandates human-subjects training and forbids any attempt at re-identification. The original IRBs at Beth Israel Deaconess Medical Center and MIT approved the data release with a waiver of informed consent and determined that secondary analyses of these de-identified records are exempt from ongoing review. Our usage strictly adheres to these terms and remains within a research-only context. The patient self-reports we generate via ChatGPT are synthetic paraphrases of those de-identified notes and contain no additional private information, so no new consent is required.

Appendix J. Acknowledgements

We used ChatGPT (gpt-4o-mini) as a writing assistant to help polish sentence structure and improve readability. All technical content, analyses, and conclusions were developed solely by the authors.

Appendix K. Limitations

Despite its contributions, our work has several important limitations.

Synthetic self-reports Our patient narratives are generated by prompting ChatGPT to paraphrase de-identified discharge text. Although we carefully instructed the model to retain only subjective symptom language, this process may introduce artifacts, omit subtle nuances, or diverge from how real patients describe their own experiences. Future work should validate our synthetic reports against authentic patient-provided narratives.

Table 10: Per-disease Top-5 Hit Rate across models.

Disease	MA	ML	MG	AM-3B	AM-7B	MF-7B	MF-8B
hepatic encephalopathy	100	46.8	53.2	2.1	100	55.3	2.1
incisional hernia	100	100	8.3	25	100	77.1	100
leiomyoma of uterus	100	100	74	98	98	96	100
malignant neoplasms of thyroid gland	100	100	80	100	97.1	94.3	97.1
other specified mood disorders	100	100	100	0	100	35.7	100
obesity	99.2	100	99.2	97.7	99.2	99.2	100
osteoarthritis of knee	98.7	99.2	100	95.4	95.8	98.7	98.7
hyperplasia of prostate	98.4	96.8	85.7	92.1	98.4	88.9	96.8
osteoarthritis of hip	98.3	100	100	86.4	96.6	98.3	91.5
fracture of neck	98.2	98.2	100	86	42.1	98.2	100
type 1 diabetes mellitus	97.9	83.3	0	68.8	91.7	8.3	87.5
recurrent depressive disorder	97.6	78	51.2	68.3	100	85.4	100
chronic pancreatitis	97.4	94.9	56.4	46.2	79.5	76.9	87.2
diarrhoea	97.4	92.1	100	7.9	100	0	97.4
intervertebral disc degeneration	97.4	93.4	0	57.9	97.4	96.1	82.9
depressive disorders, unspecified	97	75.8	63.6	100	97	0	81.8
bacterial cellulitis, erysipelas or lymphangitis	96.8	34.9	0.4	0	86.6	38.7	36.6
calculus of ureter	96.6	86.2	74.1	75.9	96.6	46.6	81
degenerative condition of spine, unspecified	96.5	77.2	100	12.3	87.7	8.8	47.4
cerebral ischaemic stroke due to embolic occlusion	96.3	11	0	26.6	93.6	0	0
left ventricular failure with reduced ejection fraction	96.3	0.8	0	20.1	76.6	77.9	77.5
calculus of kidney	96.2	92.5	100	73.6	88.7	60.4	88.7
traumatic subdural hemorrhage	96.2	71.7	50.9	0	77.4	0	66
alcoholic liver disease	95.5	93.2	45.5	84.1	90.9	15.9	95.5
malignant neoplasms of prostate	95.3	90.6	1.6	76.6	84.4	81.3	79.7
diverticulosis of large intestine	95.2	88.1	11.9	35.7	69	85.7	83.3
left ventricular failure with preserved ejection fraction	95.2	11	0	25.7	93.4	57.7	82.7
ventricular tachycardia	95.1	84	64.2	0	86.4	76.5	77.8
coronary atherosclerosis	94.8	91.6	76.6	25.1	59.6	0	48.6
cerebral ischaemic stroke	94.7	63.3	0	0	51.3	0	31.3
fracture of femur	94.3	94.3	97.1	2.9	11.4	94.3	97.1
intracerebral haemorrhage	94.3	69.5	10.5	0	75.2	0	52.4
malignant neoplasm metastasis in bone or bone marrow	94.3	20	0	0	28.6	0	31.4
asymptomatic stenosis of intracranial or extracranial artery	93.8	64.1	64.1	71.9	87.5	6.3	67.2
cerebral aneurysm, nonruptured	93.7	79.3	7.2	73.9	80.2	6.3	83.8
malignant neoplasm metastasis in spinal cord	93.2	1.1	15.9	0	37.5	0	8
disorders due to use of alcohol	92.9	0	0	0	100	53.6	10.7
chronic obstructive pulmonary disease	92.7	55.2	0	20.8	71.8	50.2	34.7

<i>(continued)</i> disease	MA	ML	MG	AM-3B	AM-7B	MF-7B	MF-8B
calculus of bile duct without cholangitis or cholecystitis	92.5	0	0	0	75	52.5	0
alcohol withdrawal	92	100	95.4	96.6	94.3	96.6	96.6
obstruction of large intestine	91.9	92.7	99.2	21.8	94.4	93.5	78.2
malignant neoplasms of kidney, except renal pelvis	91.9	48.6	43.2	62.2	75.7	48.6	73
diverticulitis of large intestine	91.6	39.6	6.4	31.7	99.5	57.4	28.7
aortic valve stenosis	91.5	40.6	100	77.4	15.1	77.4	79.2
fracture of lumbar vertebra	91.4	77.1	88.6	14.3	17.1	82.9	77.1
macro reentrant atrial tachycardia	90.9	72.7	9.1	24.2	93.9	30.3	75.8
cholelithiasis	90.6	68.8	0	6.3	18.8	56.3	28.1
alcoholic cirrhosis of liver without hepatitis	90.6	9.4	54.7	100	56.6	94.3	37.7
acute appendicitis	90.2	93.4	18.9	70.5	91.8	85.2	82.8
epilepsy or seizures, unspecified	89.1	87	80.4	100	93.5	0	84.8
abdominal aortic aneurysm	88.9	71.1	66.7	48.9	77.8	22.2	77.8
hepatic fibrosis or cirrhosis	88.9	7.4	81.5	0	48.1	0	0
crohn disease	88.5	88.5	80.8	57.7	80.8	76.9	88.5
influenza, virus not identified	88.5	61.5	7.7	38.5	92.3	0	50
transient ischaemic attack	88.2	80.4	43.1	0	100	7.8	92.2
schizoaffective disorder	87.9	45.5	9.1	0	27.3	39.4	87.9
acute myocardial infarction	87.5	83.3	0	12.5	95.8	16.7	95.8
acute upper respiratory infections of unspecified site	87.5	65	77.5	50	42.5	82.5	10
malignant neoplasm of pancreas	87.1	17.7	4.8	0	56.5	33.9	45.2
asthma	86.4	100	93.2	100	98.3	98.3	100
type 2 diabetes mellitus	86.2	64.2	0	36.6	63.4	2.4	76.4
traumatic subdural haemorrhage	85.3	35.8	15.8	0	69.5	0	33.7
malignant neoplasms of bronchus or lung	85	32.5	30	22.5	75	2.5	35
acute nonst elevation myocardial infarction	84.8	49.5	0	13.6	64.1	58.6	25.3
intestinal infections due to clostridioides difficile	83.7	4.7	0	0	36	0	7
anaemias or other erythrocyte disorders, unspecified	83.3	11.1	0	8.3	44.4	8.3	25
subarachnoid haemorrhage	83.3	64.8	0	0	9.3	0	77.8
obstruction of bile duct	82.5	43.3	78.4	3.1	63.9	24.7	36.1
gastrointestinal bleeding	82.3	86.1	0	50.6	89.9	65.8	70.9
malignant neoplasm metastasis in retroperitoneum	82.2	4.4	2.2	0	8.9	4.4	11.1
cholangitis	81.9	80.7	6	49.4	74.7	79.5	90.4
pathological fracture	81.8	93.9	6.1	60.6	78.8	3	87.9
single episode depressive disorder	81.2	94.1	18.8	92.9	96.5	98.8	100
malignant neoplasm of liver	81	69	0	0	14.3	47.6	69
pneumonitis due to solids or liquids	80.7	21.1	0	0	8.8	1.8	1.2
multiple valve disease	80.2	77.2	3.1	77.2	83.3	87.7	90.1
schizophrenia or other primary psychotic disorders, unspecified	80	2	20	88	38	0	6

<i>(continued)</i> disease	MA	ML	MG	AM-3B	AM-7B	MF-7B	MF-8B
functional nausea or vomiting	79.6	55.6	98.1	68.5	88.9	90.7	98.1
hypertensive renal disease	79.5	79.5	40.9	54.5	45.5	79.5	70.5
complete atrioventricular block	79.2	70.8	0	27.1	79.2	31.3	91.7
constipation	78.8	90.4	75	26.9	92.3	50	98.1
acute cholecystitis	78.8	52.5	0	2	70.7	39.4	23.2
iron deficiency anaemia	78.8	81.8	0	27.3	45.5	90.9	84.8
hypertensive heart disease	78.7	37.4	0.3	0.3	21	10.2	3
gastroenteritis or colitis without specification of infectious agent	78.3	2.1	0	0	33.6	0	0
acute pancreatitis	78.3	92.2	42.2	58.1	83.7	53.9	89.5
viral intestinal infections, unspecified	77.8	2.8	0	5.6	38.9	77.8	0
acute posthaemorrhagic anaemia	75	57.7	0	0	63.5	17.3	30.8
gastrooesophageal reflux disease	74.3	28.6	0	20	85.7	0	22.9
peritonitis	74.1	74.1	0	29.6	96.3	51.9	70.4
atrial fibrillation	73.5	87.4	5.5	18.7	77.4	55.5	71
encephalopathy due to toxicity	73.2	7	0	2.8	40.8	28.2	8.5
sepsis without septic shock	72.9	14.2	10.7	0	47.4	17.8	20.1
multiple sclerosis	71.9	100	75	87.5	81.3	96.9	96.9
malignant neoplasm metastasis in brain	71.1	7.9	15.8	10.5	7.9	0	68.4
primary neoplasms of meninges	69.4	63.9	52.8	33.3	72.2	72.2	58.3
human immunodeficiency virus disease	69.2	36.5	0	0	19.2	32.7	5.8
without mention of tuberculosis or malaria							
orthostatic hypotension	69.1	70.2	13.8	1.1	78.7	43.6	23.4
hypo-osmolality or hyponatraemia	69.1	16.5	0	0	17.5	0	4.1
acute pyelonephritis	65.5	69	0	0	72.4	37.9	65.5
neutropaenia	61.5	89.2	0	36.9	90.8	46.2	86.2
venous thromboembolism	59.4	56.5	47.8	34.8	43.5	33.3	71
hypotension, unspecified	56.8	18.9	100	100	29.7	83.8	0
other specified cardiac arrhythmia	56.2	46.6	0	0	45.2	2.7	47.9
pulmonary thromboembolism	56	46.6	1.6	11.9	41.5	0	37.8
urinary tract infection, site not specified	55.9	31.2	0	0.8	45.9	19.9	0.5
hyperkalaemia	52.2	73.9	21.7	0	69.6	69.6	69.6
deep bacterial folliculitis or pyogenic abscess of the skin	49.2	37.3	0	94.9	98.3	15.3	74.6
acute respiratory failure	47.5	90.7	0.8	61.9	86.4	83.9	93.2
essential hypertension	39.5	81.6	0	21.1	47.4	10.5	94.7
pleural effusion	38.6	59.1	34.1	4.5	54.5	27.3	47.7
pneumonia	37.8	96.1	68.2	92.6	89.1	74.5	93.2
bacterial pneumonia	35.9	84.6	7.7	48.7	38.5	100	100
congestive heart failure	30.1	80.7	0	0	77.1	1.2	18.1
bacteraemia	17.9	24.4	14.1	0	15.4	6.4	5.1
dehydration	6.1	92.1	94.7	43	88.6	70.2	96.5
chronic kidney disease	4.6	50.4	0.4	7.3	13.5	18.8	13.5
acute kidney failure	3.2	30.8	0.6	27.8	30	26.4	64.2